doi:10.2109/jcersj2.122.317

Low-temperature synthesis of oriented CoPtCu–MgO and CoFePt–Ag–SiO_2 nanocomposite thin films by rf-magnetron sputtering

Kazuhisa SATO, Tamotsu KOSAKA* and Toyohiko J. KONNO

Institute for Materials Research, Tohoku University, Sendai 980–8577, Japan
***Department of Materials Science, Tohoku University, Sendai 980–8579, Japan**

Journal of the Ceramic Society of Japan 122 [5] 317-321 2014 Reprint

Journal of the Ceramic Society of Japan 122 [5] 317-321 2014 Paper

Low-temperature synthesis of oriented CoPtCu–MgO and CoFePt–Ag–SiO_2 nanocomposite thin films by rf-magnetron sputtering

Kazuhisa SATO,† Tamotsu KOSAKA* and Toyohiko J. KONNO

Institute for Materials Research, Tohoku University, Sendai 980–8577, Japan
***Department of Materials Science, Tohoku University, Sendai 980–8579, Japan**

Nanocomposite thin films composed of oriented $Co_{50}Pt_{44}Cu_6$ nanoparticles embedded in a MgO matrix has been synthesized by rf-magnetron co-sputtering onto NaCl(001) substrates kept at 620 K. As the sputtering power increases, (001) orientation is improved and atomic ordering is also promoted. However, superlattice reflections are quite weak and the ordered region is limited in local area of the nanoparticles, indicating low degree of order. Electron diffraction and elemental mapping revealed that additive Cu is alloyed with CoPt. We have also fabricated $(Co_{26}Fe_{20})Pt_{44}$–Ag_{10}–SiO_2 nanocomposite thin films at 675 K for comparison. Atomic ordering is promoted by Fe and Ag addition as well as higher substrate temperature; however, it was found that ternary element (Cu, Ag, Fe) addition into CoPt alloy is not so effective to promote atomic ordering. Origin of the slow ordering kinetics is discussed using thermodynamical parameters.

Key-words : CoPtCu–MgO, CoFePt–Ag–SiO_2, Nanoparticle, Sputtering, Kinetic ordering temperature, Transmission electron microscopy

[Received November 29, 2013; Accepted February 1, 2014]

1. Introduction

Recent demands for ultrahigh density magnetic storage technology require the development of recording media with higher magnetocrystalline anisotropy energy (MAE) in order to ensure thermal stability of magnetization as well as ultrahigh recording density.[1)–4)] For such a purpose, equiatomic CoPt alloy nanoparticles are one of the candidate materials.[5)–7)] The hard magnetic properties of this alloy is attributed to the tetragonal $L1_0$-type ordered structure, which is composed of alternate stacking of Co(001) and Pt(001) atomic planes in the [001] direction.[8),9)] It is also noted that the MAE is dependent on the degree of order (long-range order) of the $L1_0$-type ordered structure.

It has been reported that kinetic ordering temperature of the equiatomic CoPt alloy is much higher than that of other similar compounds such as FePd or FePt.[10)] Actually, a high coercivities exceeding 240 kA/m have been obtained at 300 K for 10 nm-sized FePd and FePt nanoparticles after annealing at 873 K. In contrast, CoPt nanoparticles showed only 21 kA/m after high temperature annealing as high as 1023 K for 3.6 ks.[10)] Therefore, formation of the ordered CoPt phase at a reduced temperature is the key issue for practical applications. However, in spite of several attempts in order to reduce the kinetic ordering temperature of the CoPt nanoparticles,[11)] no report has succeeded in effectively reducing the kinetic ordering temperature.

One of the authors has demonstrated that kinetic ordering temperature of FePt nanoparticles can be largely reduced by rf-magnetron co-sputtering of Fe, Pt, and Cu onto heated NaCl(001) substrates.[12)] Actually, atomic ordering, epitaxial growth, high areal-density dispersion, and high coercivity (111 kA/m at 300 K) have been achieved for ternary $Fe_{37}Pt_{51}Cu_{12}$ nanoparticles at a reduced substrate temperature as low as 613 K. Thus, a combination of co-sputtering and a ternary element addition is expected to be a promising way for low temperature synthesis of the ordered CoPt nanoparticles.

In this study, we hence intend to apply the aforementioned technique to the growth of CoPt nanoparticles with additive elements (Cu, Fe, and Ag). Structure and composition of the CoPt-based ternary alloy nanoparticles were examined by using (scanning) transmission electron microscopy [(S)TEM] and electron diffraction.

2. Experimental procedure

Thin films of CoPtCu ternary alloy nanoparticles were synthesized by co-deposition of Co (99.98%), Pt (99.95%), and Cu (99.96%) targets using rf-magnetron sputtering onto NaCl(001) substrates cleaved in air. The sputtering was performed in Ar (99.999%) gas at a pressure of 1.33–11.97 Pa with a chamber base pressure of 2×10^{-6} Pa. Particle size and particle density were changed by controlling the sputtering power (30–90 W) and sputtering duration (30–70 s). Substrate temperatures were changed between 600 and 700 K. After the co-sputtering of CoPtCu, surface of the nanoparticles were coated by MgO thin films sputtered under Ar+O_2 gas flow (oxygen content of 25%). Using the same experimental setup, we also prepared CoFePt–Ag–SiO_2 nanocomposite thin films for comparison. Pure Fe (99.99%) and Ag (99.98%) were used for co-sputtering in addition to Co and Pt. The specimen films were removed from the NaCl substrate by immersing the substrate in distilled water, and then floating films were mounted onto Cu or Mo microgrids for

† Corresponding author: K. Sato; E-mail: ksato@imr.tohoku.ac.jp
‡ This article was selected from the presentations at "STAC-7" (The 7th International Conference on the Science and Technology for Advanced Ceramics) held in Yokohama, Japan (2013), through the regular reviewing procedure.

DOI http://dx.doi.org/10.2109/jcersj2.122.317

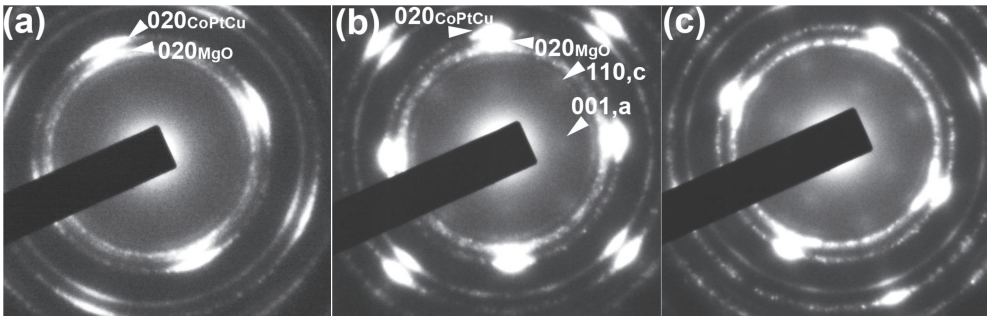

Fig. 1. SAED patterns of the $Co_{50}Pt_{44}Cu_6$–MgO nanocomposite thin films sputtered at 620 K. The sputtering power is as follows: (a) 30 W, (b) 60 W, and (c) 90 W.

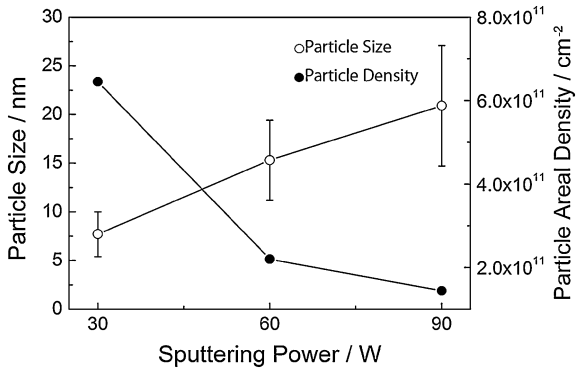

Fig. 2. Sputtering power dependence of mean particle size and particle areal density of the $Co_{50}Pt_{44}Cu_6$–MgO nanocomposite thin films deposited at 620 K.

electron transparency.

The structure and morphology of the prepared nanocomposite thin films were characterized using a JEOL JEM-3011 TEM (300 kV) and an FEI Titan80-300 (S)TEM (300 kV) equipped with a CEOS aberration corrector for the objective lens. Alloy composition was determined by energy dispersive X-ray spectrometry (EDS) attached to the (S)TEM. Magnetic properties were measured using a superconducting quantum interference device magnetometer (Quantum Design, MPMS-XL) with magnetic fields up to 2.39 MA/m.

3. Results

3.1 CoPtCu–MgO nanocomposite thin films

Figure 1 shows selected area electron diffraction (SAED) patterns of CoPtCu–MgO nanocomposite thin films deposited at 620 K with a sputtering duration of 45 s. The sputtering power was set to (a) 30 W, (b) 60 W, and (c) 90 W with Ar gas pressure of 1.33 Pa. Reflections of both CoPtCu and MgO are clearly seen in the SAED patterns. As the sputtering power increases, (001)-oriented growth of the CoPtCu nanoparticles develops and also atomic ordering is promoted as noticed by appearance of weak superlattice reflections. Note that 001 and 110 superlattice reflections, as indicated by arrowheads, correspond to the $L1_0$ ordered domain with the *c*-axis oriented parallel (a-, or b-domain) and normal (c-domain) to the substrate surface. The increase of kinetic energy of sputtered ions enhances atomic migration on the substrate surface, which may contribute to the promotion of epitaxial growth and atomic ordering.

Figure 2 shows average particle size (open circle) and particle areal density (solid circle) of the films as a function of the sputtering power. As the sputtering power increases, particles grow due to the increase of sputtering rate, which can be explained by the enhancement of plasma density. The mean particle size increases from 7.7 nm ($\sigma = 2.3$ nm) to 20.9 nm ($\sigma = 6.2$ nm), while the particle density reduces from 6.5×10^{11} to 1.4×10^{11} cm^{-2}. Hereafter, we focus on the microstructure of a specimen prepared at 60 W.

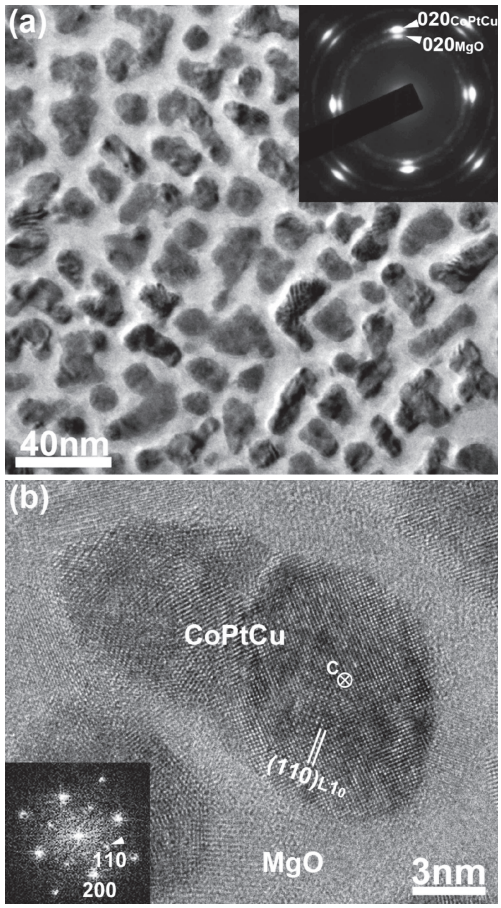

Fig. 3. (a) BF-TEM image and the corresponding SAED pattern of the $Co_{50}Pt_{44}Cu_6$–MgO nanocomposite thin film deposited at 620 K with a sputtering power of 60 W. (b) HRTEM image and the corresponding FFT pattern of a CoPtCu nanoparticle.

Figure 3(a) shows a bright-field (BF) TEM image and the corresponding SAED pattern of the CoPtCu–MgO nanocomposite thin films sputtered at 60 W. Alloy nanoparticles are separated by the oxide coating film. The average particle size is 15.3 nm ($\sigma = 4.1$ nm) with particle areal density of 2.2×10^{11} cm^{-2}.

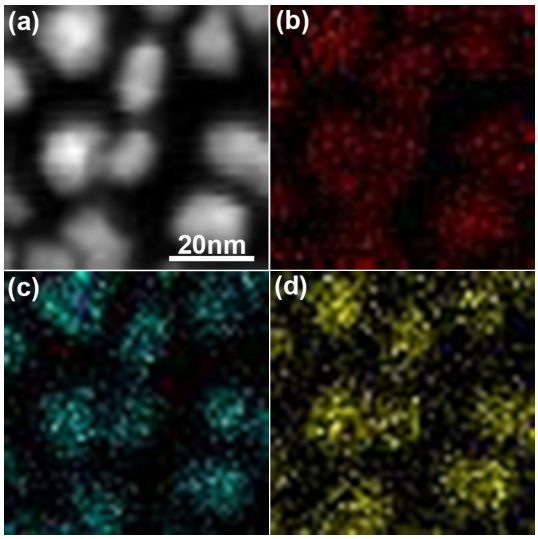

Fig. 4. STEM-EDS elemental maps of the $Co_{50}Pt_{44}Cu_6$–MgO nanocomposite thin film formed at 620 K with a sputtering power of 60 W: (a) HAADF-STEM image, (b) Co-K map, (c) Pt-L map, and (d) Cu-K map.

According to the TEM-EDS analysis, the average alloy composition evaluated was Co-44 at %Pt-6 at %Cu assuming theoretical k-factors. We can estimate statistical errors of the integrated intensities of characteristic X-ray ($\sqrt{N}/N$, N: integrated intensity) to be at most 1% within the present experimental condition. In the SAED pattern, growth of (001)-oriented CoPtCu nanoparticles is seen, although weak diffraction rings still remain. The pattern shows a tendency of cube-on-cube orientation between CoPtCu nanoparticles and the MgO cover layer. According to our previous study on CoPt nanoparticles epitaxially grown on NaCl(001) substrates,[13] cube-on-cube orientation relationship also exists between CoPt and NaCl in spite of a large lattice mismatch of 32% ($a_{CoPt} = 0.3806$ nm, $a_{NaCl} = 0.5628$ nm). This can be explained by a coincidence cell of 3(CoPt):2(NaCl), which gives a mismatch of -1.4%.[14]

Figure 3(b) shows a high-resolution TEM (HRTEM) image and the corresponding Fast Fourier Transform (FFT) pattern of a CoPtCu nanoparticle. The $L1_0$ ordered region is seen in the HRTEM image as characterized by (110) lattice fringes of the ordered structure. Attached FFT pattern taken from the ordered area also includes 110 superlattice reflections. The ordered region is limited in a local area of the particle and adjacent area shows crossed {200} lattice fringes of the disordered phase, indicating an intermediate stage of atomic ordering with a low degree of order.

It is considered that additive Cu is alloyed with CoPt, since no reflections of pure Cu can be seen in the SAED pattern. In the case of a bulk $L1_0$-FePtCu ternary ordered alloy, Cu substitutes Fe-site, which was determined by ALCHEMI method.[15] Thus it is presumed that Cu preferentially substitutes Co-site in the $L1_0$ ordered CoPtCu ternary alloy by the analogy from the preceding study. To check compositional inhomogeneity, we have carried out STEM-EDS elemental mapping. **Figure 4** shows (a) a high-angle annular dark-field (HAADF) STEM image, (b) Co-*K* map, (c) Pt-*L* map, and (d) Cu-*K* map (pixel size: 1.25 nm). As seen, Cu-map overlaps with the Co and Pt-maps and isolated Cu particle is not seen in this area, suggesting alloying of Cu into the CoPt phase, which corresponds to the result of electron diffraction.

We have examined the co-sputtering under higher substrate temperatures up to 650 K; however, the ordering was not sufficiently improved. Thus, it was found that Cu addition into CoPt alloy nanoparticles is not effective to promote atomic ordering, in contrast with the Cu addition into FePt nanoparticles.[12]

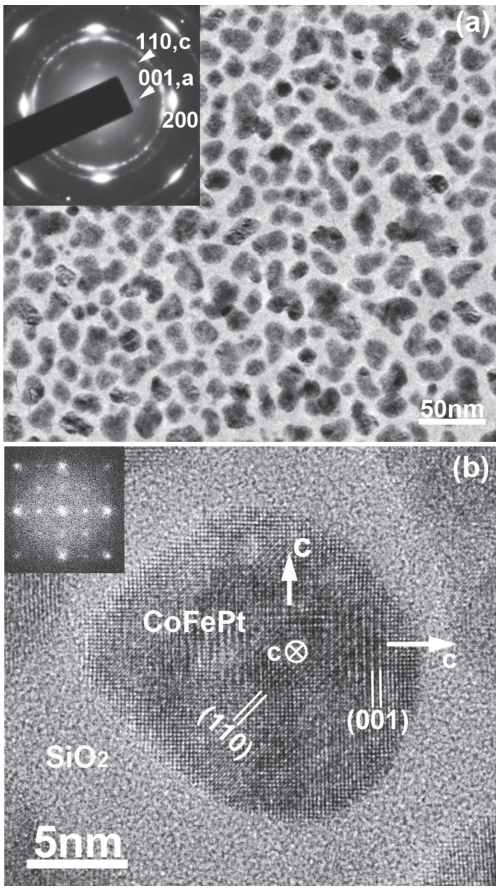

Fig. 5. (a) BF-TEM image and the corresponding SAED pattern of the $(Co_{26}Fe_{20})Pt_{44}$–Ag_{10}–SiO_2 nanocomposite thin film formed at 675 K with a sputtering power of 90 W. (b) HRTEM image and the corresponding FFT pattern of a nanoparticle with a three-variant ordered domain structure.

We also fabricated CoPtCu–SiO_2 nanocomposite thin films by using the same experimental setup. It was found that particulate microstructures as well as atomic ordering of CoPtCu nanoparticles are not practically affected by either crystalline MgO or amorphous SiO_2.

3.2 CoFePt–Ag–SiO_2 nanocomposite thin films

Besides the Cu addition, we have also examined Ag, Fe, and their simultaneous addition into CoPt nanoparticles. As a result, it was found that the atomic ordering is not effectively promoted by Ag addition under substrate temperatures less than 650 K. In the case of CoPt nanoparticles with additive Fe, atomic ordering is promoted as the Fe content increases. This effect becomes prominent for high Fe concentration specimens (>20 at %Fe) prepared at substrate temperatures higher than 650 K. When the Fe content is quite high ($Fe_{40}Co_{10}Pt_{50}$), the ordered nanoparticles were formed at 613 K and they showed a coercivity of 63 kA/m at room temperature.[16] The promotion of atomic ordering by Fe-addition can be explained by the increase of the themodynamical ordering temperature by Fe addition, which will be discussed in later. In this study we found that Fe addition enhances particle growth and faceting of particle shape, while these two effects

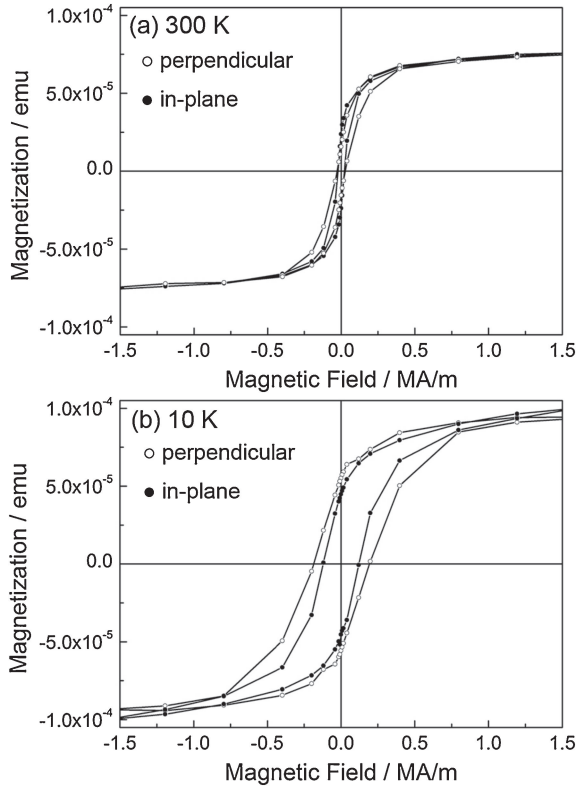

Fig. 6. Magnetization curves of the $(Co_{26}Fe_{20})Pt_{44}$–Ag_{10}–SiO_2 nanocomposite thin film measured at (a) 300 K and (b) 10 K. Open and solid circles indicate magnetization measured perpendicular and in-plane direction, respectively.

were suppressed by Ag addition.

Figure 5(a) shows a BF-TEM image and the corresponding SAED pattern of a typical example of $(Co_{26}Fe_{20})Pt_{44}$–Ag_{10}–SiO_2 nanocomposite thin films sputtered at 675 K (Ar gas pressure: 7.98 Pa, sputtering power: 90 W, sputtering duration: 60 s). Different from the MgO, sputtered SiO_2 forms an amorphous continuous thin film. The mean particle size is 17.9 nm ($\sigma =$ 6.6 nm) with particle areal density of 2.1×10^{11} cm^{-2}. The intensity of superlattice reflections is obviously enhanced compared with those for CoPtCu nanoparticles, indicating the promotion of atomic ordering. It should be noted that additive Ag is immiscible to CoPt or FePt.[11] An HRTEM image and the corresponding FFT pattern shown in Fig. 5(b) reveals formation of a three-variant ordered domain structure; atomic ordering is still in an intermediate stage. According to our previous study on binary FePt nanoparticles, as the atomic ordering proceeds, ordered domains disappear and a single-variant structure is formed.[17] Overall, ternary element addition (Cu, Ag, or Fe, with content of less than 15 at%) into CoPt alloy is not so effective to promote atomic ordering.

Figure 6 shows magnetization curves of the $(Co_{26}Fe_{20})Pt_{44}$–Ag_{10}–SiO_2 nanocomposite thin films measured at both 300 K (a) and 10 K (b). Note that magnetic easy axes (c-axis of the $L1_0$ structure) are in the three orthogonal directions parallel to the principal axes of NaCl, because of the (001) oriented growth of the $L1_0$-CoFePt nanoparticles on a NaCl(001) substrate. Magnetization curves measured in the film normal direction show higher coercivity than those measured in plane direction. This is due to the preferential c-axis orientation in the film normal direction. In spite of the atomic ordering as shown in Fig. 5, coercivity remained as low as 28 kA/m (perpendicular) and 21 kA/m (in-plane) at 300 K. These coercivity values are comparable to those obtained for epitaxial CoPt nanoparticles produced by electron beam deposition followed by postdeposition annealing at 1023 K.[10] In this sense, atomic ordering proceeds at quite a lower temperature; however, the coercivity values are still low. High coercivity exceeding 240 kA/m at 300 K is desired for practical applications. At 10 K, coercivity was markedly enhanced and reached 188 kA/m (perpendicular) and 121 kA/m (in-plane). Thus, the perpendicular coercivity was enhanced approximately 7 times of the room temperature value, indicating the existence of thermal fluctuation of magnetization due to a rather low MAE, which is originated from a low degree of order.

Table 1. Melting temperature (T_m), order–disorder transformation temperature (thermodynamic ordering temperature, T_c), and heat of formation (ΔH) of CoPt, FePt, FePd alloys

	T_m/K[18]	T_c/K[18]	T_c/T_m	ΔH/kJ/mol[19]
CoPt	1773	1098	0.550	−14
FePt	1853	1573	0.828	−25
				−27.2[20]
FePd	1573	1063	0.606	−9.4

4. Discussion

Table 1 shows melting temperature (T_m),[18] order–disorder transformation temperature (thermodynamic ordering temperature, T_c),[18] and heat of formation (ΔH)[19,20] of CoPt, FePt, and FePd alloys. At first, annealing temperature (T_a) normalized by T_m (namely, T_a/T_m) is a measure of diffusion coefficient via vacancy concentration, which plays an important role when atomic ordering in disordered nanoparticles are concerned. In this sense, rather low T_m of the Fe–Pd alloy is beneficial compared to Fe–Pt or Co–Pt. Actually, kinetic ordering temperature of FePd nanoparticles is 100 K lower than that of FePt nanoparticles.[21] Secondly, T_c is a measure of the ordering energy, which is the driving force for atomic ordering due to free energy difference between the ordered and the disordered phase. According to the Bragg-Williams (BW) theory,[22] the T_c is expressed as follows using ordering energy (v):

$$T_c = -\frac{4v}{k_B} \quad (v < 0) \tag{1}$$

Thus, it can be said that an alloy with a higher T_c possesses the higher ordering energy. In the case of CoPt with additive Fe, atomic ordering is promoted as the Fe content increases as stated in the previous section. This is explained by the difference of T_c; namely, T_c for FePt is much higher than that for CoPt, and actually pseudo binary phase diagram (CoPt–FePt) also shows an increase of the T_c as a function of Fe content.[23] Similarly, both Fe–Pt and Co–Pt alloys are beneficial for atomic ordering in respect of the T_c compared with Fe–Pd alloy, while the experimental results are reversed in this case; ordering in FePd nanoparticles is the fastest in spite of the fact that the heat of formation is the lowest among these alloy systems. This result suggests that the T_c is not always the determining factor for atomic ordering in alloy nanoparticles.

Then we define a parameter T_c/T_m in order to compare the ordering process of the above three kinds of alloy systems, where an alloy with higher T_c/T_m is thought to order more easily. As a result, T_c/T_m of 0.550, 0.828, and 0.606 were obtained for CoPt, FePt, and FePd alloys, respectively.[10] This estimation qualitatively explains the experimental results of slow ordering kinetics

in the CoPt nanoparticles. In contrast, the highest T_c/T_m and the large negative heat of formation for the FePt alloy correspond well to the rapid ordering at lower temperatures. Note that heat of formation is a measure for alloy phase formation.[24)]

5. Conclusion

We have studied formation and structure of CoPtCu–MgO and CoFePt–Ag–SiO_2 nanocomposite thin films using TEM, STEM and electron diffraction. The results are summarized as follows.

(1) Oriented $Co_{50}Pt_{44}Cu_6$–MgO nanocomposite thin films were synthesized by rf-magnetron co-sputtering onto NaCl(001) substrates kept at 620 K.
(2) As the sputtering power increases, (001) oriented growth is enhanced and atomic ordering is also promoted. However, superlattice reflections are quite weak and the ordered region is limited in local area of the nanoparticles.
(3) Electron diffraction and STEM-EDS elemental mapping revealed that additive Cu is alloyed with CoPt.
(4) $(Co_{26}Fe_{20})Pt_{44}$–Ag_{10}–SiO_2 nanocomposite thin films were also prepared at 675 K for comparison. Atomic ordering is promoted by Fe and Ag addition as well as higher substrate temperature; however, coercivity remained as low as 28 kA/m at 300 K.
(5) Ternary element (Cu, Ag, Fe) addition into CoPt alloy is not so effective to promote atomic ordering as in the case of previously reported FePtCu nanoparticles.
(6) Origin of the slow ordering kinetics of the CoPt nanoparticles can be explained by a small value of T_c/T_m as well as the low heat of formation.

Acknowledgments This study was partially supported by a Grant-in-Aid for Challenging Exploratory Research (No. 23651094) from the Ministry of Education, Culture, Sports, Science, and Technology, Japan. KS acknowledges financial supports from the Kato Foundation for Promotion of Science and the Murata Science Foundation.

References

1) D. Weller and M. F. Doerner, *Annu. Rev. Mater. Sci.*, 30, 611–644 (2000).
2) T. Oikawa, M. Nakamura, H. Uwazumi, T. Shimatsu, H. Muraoka and Y. Nakamura, *IEEE Trans. Magn.*, 38, 1976–1978 (2002).
3) B. D. Terris and T. Thomson, *J. Phys. D Appl. Phys.*, 38, R199–R222 (2005).
4) M. H. Kryder, E. C. Gage, T. W. McDaniel, W. A. Challener, R. E. Rottmayer, G. Ju, Y. Hsia and M. F. Erden, *Proc. IEEE*, 96, 1810–1835 (2008).
5) K. Coffey, M. A. Parker and J. K. Howard, *IEEE Trans. Magn.*, 31, 2737–2739 (1995).
6) M. R. Visokay and R. Sinclair, *Appl. Phys. Lett.*, 66, 1692–1694 (1995).
7) C. Chen, O. Kitakami, S. Okamoto, Y. Shimada, K. Shibata and M. Tanaka, *IEEE Trans. Magn.*, 35, 3466–3468 (1999).
8) A. Sakuma, *J. Phys. Soc. Jpn.*, 63, 3053–3058 (1994).
9) H. Shima, K. Oikawa, A. Fujita, K. Fukamichi, K. Ishida, S. Nakamura and T. Nojima, *J. Magn. Magn. Mater.*, 290–291, 566–569 (2005).
10) Y. Hirotsu and K. Sato, *J. Ceramic Proc. Res.*, 6, 236–244 (2005).
11) C. Chen, O. Kitakami and Y. Shimada, *Appl. Phys. Lett.*, 76, 3218–3220 (2000).
12) H. W. Ryu, H. Naganuma, K. Sato and Y. Hirotsu, *Jpn. J. Appl. Phys.*, 45, L608–L610 (2006).
13) K. Sato, K. Yanajima and T. J. Konno, *Thin Solid Films*, 520, 3544–3552 (2012).
14) K. Sato, J. G. Wen and J. M. Zuo, *J. Appl. Phys.*, 105, 093509 (2009).
15) Y. Hirotsu, H. W. Ryu, K. Sato and M. Ishimaru, *J. Microsc.*, 239, 94–99 (2009).
16) A. Kovács and Y. Hirotsu, *Appl. Phys., A Mater. Sci. Process.*, 93, 543–546 (2008).
17) K. Sato, B. Bian, T. Hanada and Y. Hirotsu, *Scr. Mater.*, 44, 1389–1393 (2001).
18) Binary Alloy Phase Diagrams 2nd ed., edited by T. B. Massalski, H. Okamoto, P. R. Subramanian and L. Kacprzak, ASM International, Materials Park, OH (1990).
19) F. R. de Boer, R. Boom, W. C. M. Mattens, A. R. Miedema and A. K. Niessen, Cohesion in Metals Transition Metal Alloys, North-Holland Amsterdam (1988).
20) B. Wang, D. C. Berry, Y. Chiari and K. Barmak, *J. Appl. Phys.*, 110, 013903 (2011).
21) K. Sato, B. Bian and Y. Hirotsu, *Jpn. J. Appl. Phys.*, 39, L1121–L1123 (2000).
22) W. L. Bragg and E. J. Williams, *Proc. Roy. Soc.*, A145, 699–730 (1934).
23) V. Raghavan, The Co-Fe-Pt System, in ASM Alloy Phase Diagrams Center, ID No. 2000098, H. Okamoto and K. Cenzual (ed.), ASM International, Materials Park, OH, USA (2006–2013).
24) T. J. Konno, S. Yamamuro and K. Sumiyama, *J. Vac. Sci. Technol., B*, 20, 834–842 (2002).